https://doi.org/10.5194/egusphere-2024-1760
Preprint. Discussion started: 26 June 2024

Brief Communication: Accurate and autonomous snow water equivalent measurements using a cosmic ray sensor on a Himalayan glacier

Navaraj Pokhrel[1,2], Patrick Wagnon[1], Fanny Brun[1], Arbindra Khadka[1,2,3], Tom Matthews[4], Audrey Goutard[1], Dibas Shrestha[2], Baker Perry[5], Marion Réveillet[1]

[1]Univ. Grenoble Alpes, IRD, CNRS, INRAE, Grenoble INP, IGE, Grenoble, France
[2]Central Department of Hydrology and Meteorology, Tribhuvan University, Kirtipur, Nepal
[3]International Centre for Integrated Mountain Development, Kathmandu, Nepal
[4]Department of Geography, King's College London, London, United Kingdom
[5]Department of Geography and Planning, Appalachian State University, Boone, North Carolina, USA

Correspondence to: Navaraj Pokhrel (Navaraj.77558@cdhm.tu.edu.np)

Abstract. We analyze snow water equivalent (SWE) measurements from a cosmic ray sensor (CRS) on the lower accumulation area of Mera Glacier (Central Himalaya, Nepal) between November 2019 and November 2021. The CRS aligned well with field observations and revealed accumulation in pre-monsoon and monsoon, followed by ablation in post-monsoon and winter. COSIPY simulations suggest significant surface melting, water percolation and refreezing within the snowpack, consistent with CRS observations, yet liable to be missed by surface mass balance surveys. We conclude that CRS can be used to complement more resource-intensive manual measurements to determine mass fluxes on remote, high-altitude Himalayan glaciers.

1 Introduction

Seasonal snowpack in high mountain regions is crucial for glaciology, hydrology and climate change research (Gugerli et al., 2019). Snow accumulation and more generally high-altitude precipitation are major unknowns of the water cycle in the higher Himalayas (> 5000 m a.s.l.) (Immerzeel et al., 2015). Moreover, the quantitative assessment of snow water equivalent (SWE) in high-altitude snowpacks is vital for mitigating disaster risks, especially for floods and avalanches. In the logistically demanding environment of the higher Himalayas, accurate precipitation measurement and quantification of snow distribution are challenging, limiting reliable and continuous SWE measurements (Shea et al., 2015). The observational difficulties are compounded by high spatial heterogeneity in precipitation, driven by the complex interactions between topography and atmospheric circulation (Perry et al., 2020). There is hence a high incentive to overcome the logistical challenges and increase the density and quality of continuous SWE measurements.

https://doi.org/10.5194/egusphere-2024-1760
Preprint. Discussion started: 26 June 2024

A variety of techniques ranging from on-site measurements like snow pillows, snow pits, ground-penetrating radar to remote sensing tools like passive microwave and synthetic aperture radar, can be used to gather SWE data in remote areas, despite certain limitations and biases (Leinss et al., 2015). (Masahiro Kodama et al., 1975; Masahiro Kodama, Katsuyuki Nakai, 1979)) introduced a method using cosmic ray neutrons. These neutrons, created by cosmic rays hitting Earth's atmosphere, interact with hydrogen in water. The decrease in neutron counts upon absorption allows for the estimation of SWE values (e.g., (Gugerli et al., 2019). Measurements by cosmic ray sensors (CRS) offer autonomous, point measurements of SWE and therefore hold promise for greatly increasing the density of SWE observations in remote mountain regions.

In this study, we deployed a Hydroinnova SnowFox: a CRS able to measure SWE up to 4 meters or more (Gugerli et al., 2019; Howat et al., 2018), in the lower part of the accumulation zone of Mera Glacier (Central Himalaya, upper Dudh Koshi basin). Since 2007, Mera Glacier has undergone systematic monitoring, establishing itself as one of the longest-running field-based series concerning mass and energy balance in the Himalayas. By using field measurements, in-situ meteorological data and adjacent weather stations, alongside a surface mass and energy balance model (COSIPY), our objectives are to: (i) analyze the SnowFox performance by comparing its SWE estimating with manual field observation; (ii) understand the seasonal evolution of snowpack in the accumulation zone of Mera Glacier; and (iii) utilize COSIPY to explain the processes driving snowpack evolution within Mera Glacier's accumulation zone.

2 Study area and climate setting

Mera (27.7° N; 86.9° E; 4.84 km^2 in 2018) is a debris-free glacier in eastern Nepal's upper Dudh Koshi basin, accumulating in summer (Wagnon et al., 2021). The SnowFox was installed on a large, flat area in the lower part of Mera Glacier's accumulation zone at 5770 m a.s.l., facing north and surrounded by crevasses (Fig. 1c).

Following (Bonasoni et al., 2010), we divided the year into four distinct seasons: winter (Dec-Feb) with colder, drier, windy conditions; pre-monsoon (Mar-May) with gradually increasing temperature and humidity, and less wind; monsoon (Jun-Sep) with light wind, constantly high temperature, and heavy precipitation due to moisture influx from the Bay of Bengal; post-monsoon (Oct-Nov) with drier, sunny, colder, windier weather, and occasional typhoons causing substantial snowfall above approximately 4000 m a.s.l. within a few days, (e.g., 18-20 October 2021) (Adhikari et al., 2024). In general, vertical, and horizontal gradients of precipitation are large due to complex topography over the region (Sherpa et al., 2017). However, this spatial variability is not well quantified due to the limited number of weather stations and inter-annual variability in total precipitation.

https://doi.org/10.5194/egusphere-2024-1760
Preprint. Discussion started: 26 June 2024

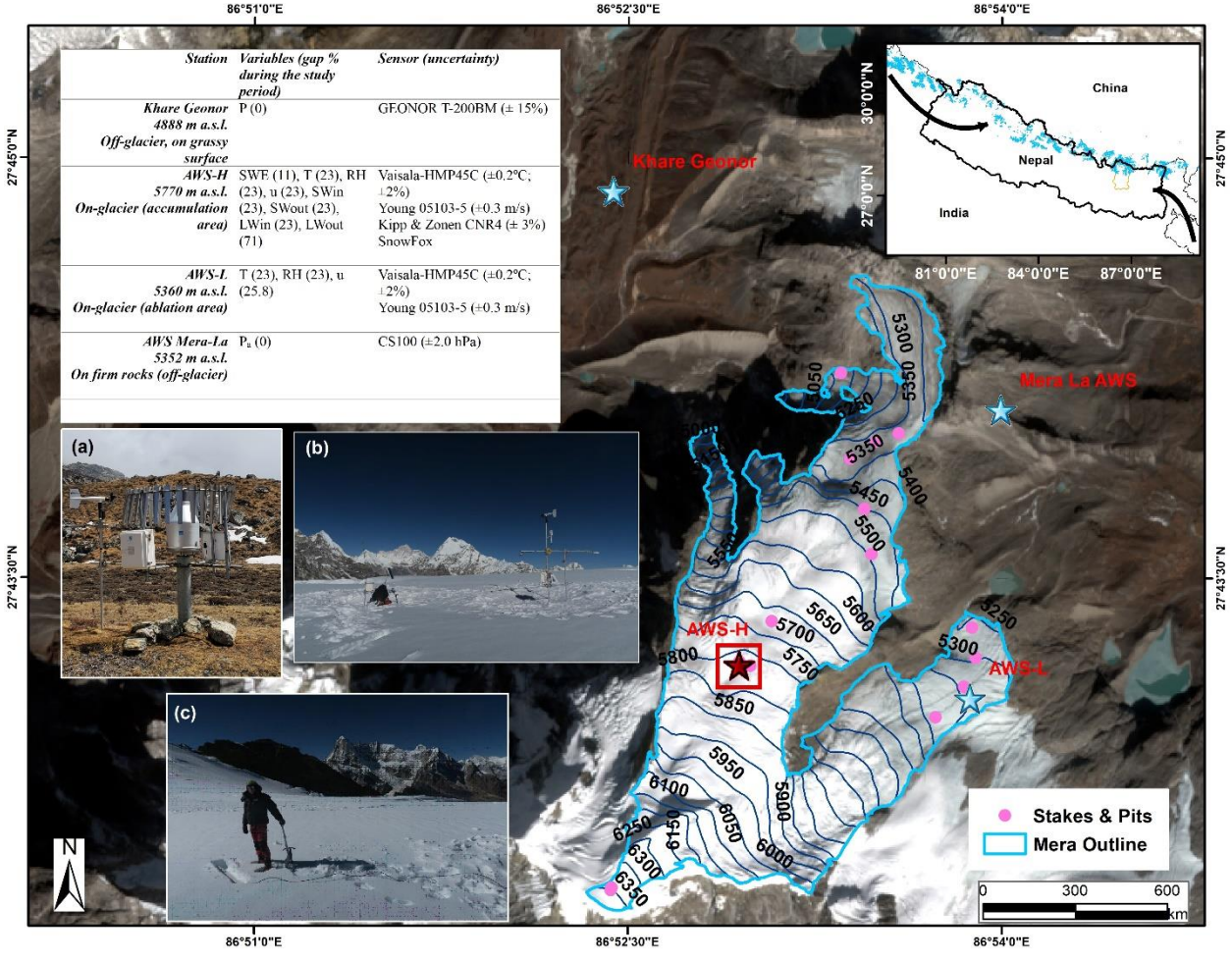

Figure 1. Map of Mera Glacier showing the network of ablation stakes and accumulation pits (pink dots). The stars represent the locations of the AWS used in this study, with in red the location of the SnowFox installed approximately 10 m northwest of AWS-H. The red square represents the grid cell at AWS-H where COSIPY simulations are done. The pictures show the all-weather Geonor precipitation gauge (a), a picture of the SnowFox site showing AWS-H on the right, the SnowFox datalogger mast on the left and the snow trench where the SnowFox is installed (in the front) (b), and the SnowFox during the installation on 12 November 2019 (c). A table (top left) provides detailed information about the stations with variables (temperature (T), precipitation (P), SWE, relative humidity (RH), wind speed (u), atmospheric pressure (P_a), outgoing longwave (LWout), incoming longwave (LWin), outgoing shortwave (SWout) and incoming shortwave radiation (SWin)), percentage of data gap for each variable, sensor types and its uncertainty. The outline of Mera Glacier is from 2018 with a total area of 4.84 km^2, and the background image corresponds to Copernicus Sentinel data (Sentinel-2 image from 24 November 2018). Elevation contours are extracted from the 2012 Pléiades DEM (Wagnon et al., 2021). The inset map gives the location of Dudh Koshi basin (yellow) in Nepal with general pathways of moisture carried by westerlies (left) and Indian summer monsoon (right). Light blue areas are the glacierized areas from Randolph glacier inventory 6 (Li et al., 2021).

3 Data and Methods

In this study, we primarily utilize data from 12 November 2019 to 21 November 2021 of two on-glacier Automated Weather Stations (AWS), namely AWS-H (equipped with SnowFox) in the accumulation area and AWS-L in the ablation area (Fig. 1). We also use data from AWS Mera-La, located off-glacier on solid rocks to fill the data gaps of the other AWSs. Additionally,

https://doi.org/10.5194/egusphere-2024-1760
Preprint. Discussion started: 26 June 2024

the Khare Geonor station records precipitation in all weather conditions (Fig. 1b). In-situ measurement of snow density and snow depth were carried out on 24 November 2020 and 19 November 2021 using snow coring with manual drilling (Wagnon et al., 2021).

On 12 November 2019, the SnowFox was installed approximately 20 cm below the fresh snow surface. The sensor counts downward falling secondary cosmic neutrons that pass through the snowpack, which is converted to SWE through a calibration function. In this case, the scanning time was 20 seconds, and the records were averaged at hourly resolution.

The corrected neutron count for time step i (N_i) is computed from the raw neutron count rate ($N_{raw,i}$) by accounting for variations in solar activity ($F_{s,i}$) and, more importantly, for changes in in-situ air pressure ($F_{p,i}$) (Gugerli et al., 2019); (Howat et al., 2018); (Jitnikovitch et al., 2021):

$$N_i = N_{raw,i}.F_{s,i}.F_{p,i} \quad (1)$$

Variations in $F_{s,i}$ are quantified with the aid of a (snow free) reference station. As there were not any neutron monitoring stations close to the study area, we used the solar correction factor established through the examination of data from 94 globally distributed, quality-controlled neutron counts station, which were found to be strongly correlated between the relative counting rates at the site of interest (Desilets, 2021) and at a reference neutron monitor center, the Jungfraujoch station (Flückiger and Bütikofer, 2009):

$$F_{s,i} = \left(1 - \frac{M_0}{M_{(t)}}(1-\tau)\right) \quad (2)$$

where, $M_{(t)}$ is the neutron count of Jungfraujoch at time t, and M_o is the counting rate at an arbitrary chosen reference time. τ is a dimensionless slope parameter adjusting the ratio to the site of interest. Its value depends on the effective cutoff rigidity (R_c) and atmospheric depth (χ), both of which respectively depend on the altitude and latitude of the site of interest ((McJannet and Desilets, 2023)):

$$\tau(\chi, R_C) = \epsilon K(c_0 + c_1\chi)[1 - \exp(-[c_2 + c_3\chi]{R_C}^{c_4+c_5\chi})] \quad (3)$$

where, K (equal to 3.08) represents a normalization factor dependent on location, while ε (equal to 1.14) denotes a correction factor that fine-tunes the sensitivity of the standard lead neutron monitor. R_c (equal to 14.53 GV) is the effective vertical rigidity calculated using the MAGNETOCOSMICS code, a part of the Geant4 toolkit available at *crnslab.org*, and χ (equal to 543.51 g cm^{-2}) is the atmospheric depth calculated using the local atmospheric pressure (P_a), and the acceleration due to gravity (g = 9.78 m s^{-2}):

$$\chi = \frac{10P_a}{g} \quad (4)$$

https://doi.org/10.5194/egusphere-2024-1760
Preprint. Discussion started: 26 June 2024

Similarly, the following barometric pressure coefficients c_0 (7.977 × 10^4), c_1 (1.626), c_2 (3.990 × 10^{-03}), c_3 (5.476), c_4 (-1.527 × 10^4), c_5 (1.250) are used respectively (Desilets, 2021). In our application, we therefore find that τ has a value of 0.324.

Air pressure is not measured directly at the study site; instead it is reconstructed based on the Mera La station using the hydrostatic equation (Wallace and Hobbs, 2006). Finally, the pressure correction factor $F_{p,i}$ is obtained by:

$$F_{p,i} = exp\left(\frac{P_i - P_0}{L}\right) \quad (5)$$

The observed hourly air pressure values are represented by P_i while P_0 stands for a reference pressure. For the reference period, we chose a long-term (12 November 2019 to 21 September 2021) mean pressure value (531.6 hPa), used also in equation 4. The mass attenuation length (L) is taken as 150 hPa for our study site based on Jungfraujoch reference station (Mcjannet and Desilets, 2022).

To calculate SWE, we used the relative neutron count ($N_{rel,i}$) i.e., the corrected neutron count (N_i) divided by a reference count (N_o=*150*) which is the averaged raw neutron count calculated from 1-minute means over 1-s time interval, between 11:00 and 12:00, local time, on 19 November 2021 while the sensor was running on-site, at the surface, after being excavated the day before. During this 1-hr run, the weather was cold and overcast, with very light snowfall. The relative neutron count is then used to derive SWE with the nonlinear equation:

$$SWE_i = -\frac{1}{\Lambda_i}.ln\, N_{rel,i} \quad (6)$$

The variable Λ_i is the effective attenuation length (in cm) with empirical values representative of a 'glacier landscape' (Λ_{min} = 14 cm, Λ_{max} = 114.1 cm, a_1 = 0.35, a_2 = 0.08 and a_3 = 1.117;(Jitnikovitch et al., 2021); (Howat et al., 2018):

$$\Lambda_i = \frac{1}{\Lambda_{max}} + \left(\frac{1}{\Lambda_{min}} - \frac{1}{\Lambda_{max}}\right).\left(1 + exp\left(\frac{a_1 - N_{rel,i}}{a_2}\right)\right)^{-a_3} \quad (7)$$

SWE measurements are compared with COSIPY mass flux simulations performed by Khadka et al. (2024) for the 0.003°×0.003° (0.01 km^2) grid cell where the SnowFox and AWS-H are located (Fig. 1). These COPSIPY simulations were forced by in-situ atmospheric measurements recorded at AWS-L and have been previously validated against all available field measurements including albedo, surface temperature and point mass balances at the AWS-H site. The input precipitation is taken from Khare station without applying any altitudinal gradient.

4 Results and discussion

The SnowFox demonstrated its effectiveness in accurately determining SWE using cosmic rays through good agreement with field measurements (Fig. 2a). During the sensor's installation, the SWE corresponds to 24 mm water equivalent (w.e.) from about 20 cm of fresh snow, corresponding to a snow density of 120 kg m^{-3}. On 24 November 2020, the sensor recorded a SWE of 562 mm w.e., closely matching the manually measured SWE of 533 ± 49 mm w.e., performed a few meters from the

https://doi.org/10.5194/egusphere-2024-1760
Preprint. Discussion started: 26 June 2024

SnowFox location. The sensor was non-functional between 3 and 24 November 2020, because the solar panel was buried by snow; and it ceased functioning on 16 September 2021, for the same reason. At that time, the cumulative SWE measured by the sensor was 1282 mm w.e. The sensor was excavated on 18 November 2021, and manually measured SWE was equal to 1357 ± 88 mm w.e. During the first operational gap, 6 mm w.e. of precipitation was recorded at the Khare Geonor station, while 137 mm w.e. was recorded during the second gap.

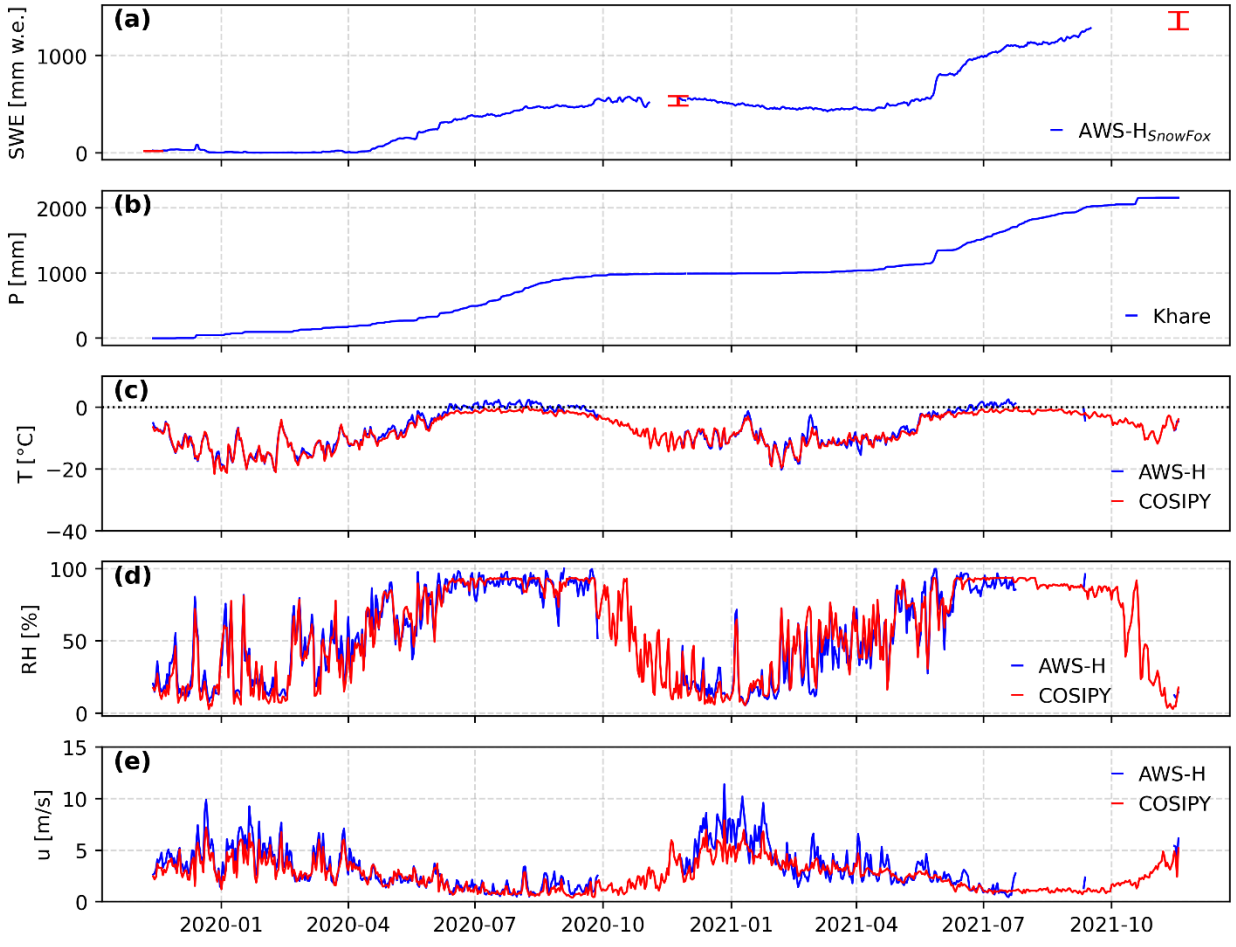

Figure 2. Daily values of (a) Cumulative SWE measured by SnowFox (blue line) and manual field measurements with error bars (in red), (b) cumulative precipitation at Khare, (c-d-e) air temperature, relative humidity, and wind speed, respectively, measured at AWS-H (blue) and used to force COSIPY at the corresponding grid cell (red) (see Khadka et al. (2024) for details). The black dashed line in panel c corresponds to T = 0°C.

Figure 2a clearly identifies a seasonal pattern in snowpack formation, with accumulation during the pre-monsoon and monsoon, typically characterized by regular snowfall, higher air temperatures (Fig. 2c), increasing relative humidity (Fig. 2d), and decreasing wind speeds (Fig. 2e). Between 12 November 2019 and 24 November 2020, the snowpack accumulated 540 mm w.e., while between 24 November 2020 and 18 November 2021, it accumulated slightly more with 742 mm w.e. This

https://doi.org/10.5194/egusphere-2024-1760
Preprint. Discussion started: 26 June 2024

larger total amount in 2021 can be attributed to the occurrence of two typhoons, Tauktae and Yaas, on 18 May and 29 May 2020, respectively, which contributed 215 mm w.e. precipitation at Khare station and 181 mm w.e. of SWE at AWS-H. Conversely, SWE tends to decrease during the post-monsoon and winter due to the low air temperatures, lower humidity, and higher winds driving increased snow sublimation and wind erosion. A spectacular example of such processes was observed on 14 December 2019: a sudden increase of 60 mm w.e. was recorded by the SnowFox, which was also captured by the Geonor gauge in Khare (Fig. 2b), with 44 mm w.e. of precipitation recorded but, within two days following this event, the SWE decreased by 40 mm w.e. due to strong winds. Subsequently, the cumulative SWE monotonically decreased and reached 1 mm w.e. by the end of February 2020.

Differences are detected between (i) the monthly cumulative precipitation at Khare; (ii) changes in SWE at AWS-H measured by the SnowFox; and (iii) the mass fluxes simulated by COSIPY (Fig. 3). During the winter months, the monthly SnowFox SWE changes are typically negative, even when accumulation is observed at Khare, which we attribute to sublimation and erosion due to strong winds (Fig 2e; (Litt et al., 2019). The simulated cumulative sublimation between November and March is as high as 93 mm w.e. and 74 mm w.e. in 2019/20 and 2020/21 respectively (67 % and 70% of annual sublimation), compared to 173 and 54 mm of total precipitation recorded at Khare (only 18 and 6% of annual precipitation). In May, June, and September, the increases in SWE measured by the SnowFox are more similar to the Khare precipitation totals.

For the core monsoon months (July-August), the two years of measurements are very different. In the first year (2019/20), the change in SWE is small compared to the precipitation at Khare (100 mm w.e. vs. 384 mm w.e.), while in the second year the values are closer (185 mm w.e. vs. 300 mm w.e.). As the COSIPY simulations show the qualitative importance of refreezing (about 80% of the meltwater), we interpret the difference as a differential refreezing efficiency, because in the second year the SnowFox was buried deeper in the snowpack (323 cm on 18 November 2021) compared to the first year (120 cm on 24 November 2020). Indeed, when the sensor is located closer to the surface (in the first year), a greater proportion of the percolating water is likely to freeze below the sensor and thus not be measured by SnowFox. This interpretation is supported by the systematic observation of ice lenses in the snowpack from the surface to several meters below during field work.

This interpretation has a major implication for field measurements, as it suggests that monsoon meltwater can percolate below the previous year's autumn horizon before freezing. Consequently, point surface mass balance measurements made in the lower part of the accumulation area of Mera Glacier (Wagnon et al., 2021) may miss some of this internal accumulation and are likely to be negatively biased. This problem may be common to summer accumulation type glaciers.

https://doi.org/10.5194/egusphere-2024-1760
Preprint. Discussion started: 26 June 2024

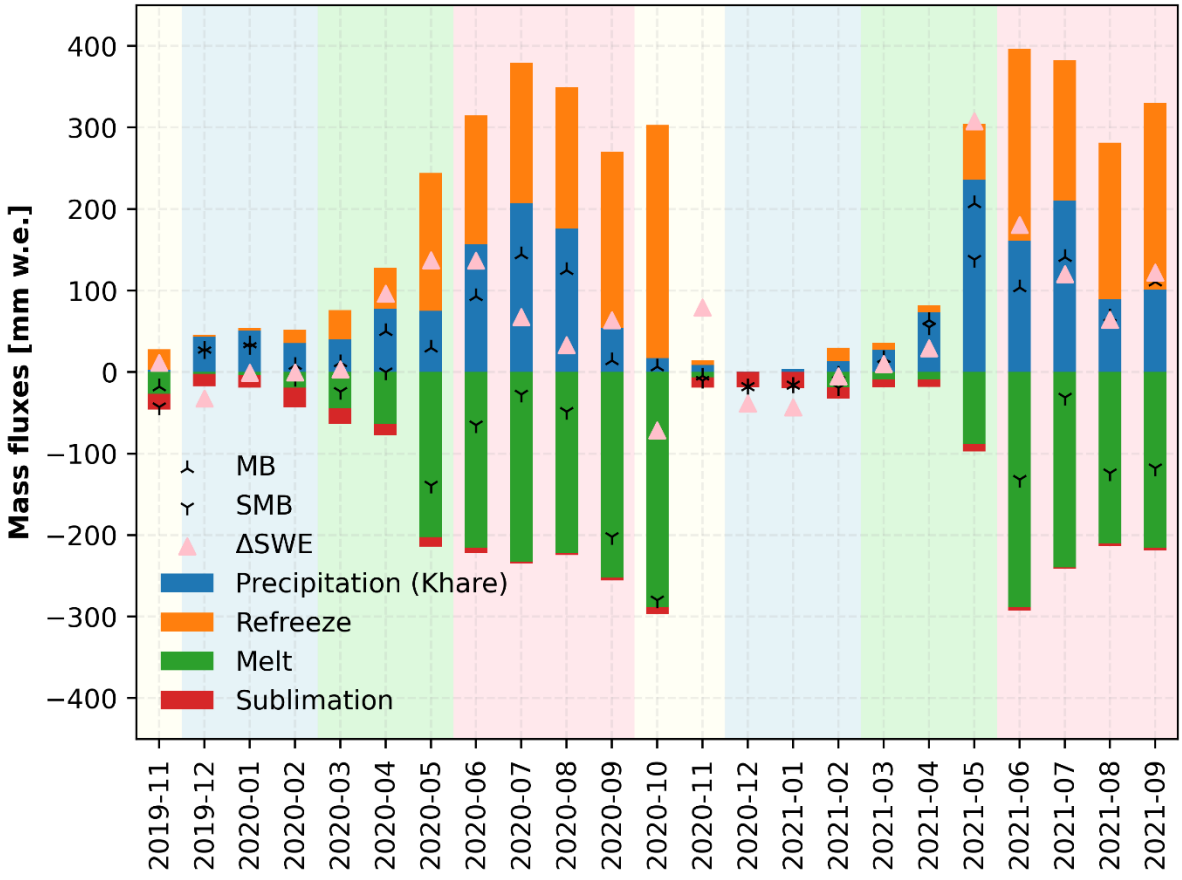

Figure 3. Monthly values of precipitation at Khare (blue bars), measured changes in SWE at AWS-H (pink triangles) and mass fluxes at the corresponding grid cell simulated by COSIPY: melt (green bars), refreezing (orange bars), sublimation (red bars), surface mass balance SMB (= precipitation + melt + sublimation) (downward black arrow) and mass balance MB (= precipitation + melt + refreezing + sublimation) (upward black arrow). Light red, yellow, blue and green shaded areas represent the monsoon, the post-monsoon, the winter and pre-monsoon, respectively.

5 Conclusions

Operating a SnowFox sensor in the accumulation zone of Mera Glacier for two years has allowed continuous monitoring of changes in SWE, which agrees well with field observations in November 2020 and 2021. Our analysis highlights seasonal variations in SWE, with accumulation occurring in the pre-monsoon and monsoon, followed by ablation in the post-monsoon and winter due to sublimation and wind erosion. Further investigation of the mass balance components using COSIPY model revealed a significant amount of meltwater percolation and refreezing within the snowpack, explaining how physical processes can contribute to the seasonal evolution of the snowpack. We conclude that the expansion of such measurements could provide

https://doi.org/10.5194/egusphere-2024-1760
Preprint. Discussion started: 26 June 2024

much improved distributed estimates of snowpack evolution and governing processes, complementing more resource-intensive manual measurements on remote, high altitude Himalayan glaciers.

6 Data availability

All data will be deposited in a repository pending publication.

7 Acknowledgements

This work has been supported by the French Service d'Observation GLACIOCLIM (part of IR OZCAR). This work would not have been possible without the International Joint Lab Water-Himal (principal investigators D. Shrestha, and P. Wagnon) supported by IRD and all the efforts from people in the field: porters, students, and helpers who are greatly acknowledged here. This research was conducted in partnership with National Geographic Society, Rolex and Tribhuvan University, with approval from all relevant agencies of the Government of Nepal.

8 Author contribution

Conceptualization: PW, FB, TM, BP; Data curation: NP, PW, AK; Formal analysis: NP; Investigation: NP, PW, FB, AK, MR, AG; Funding acquisition: PW, TM, BP; Writing (original draft): NP, PW, FB, AK, MR, AG, TM, BP

9 Competing interest

The authors declare that they have no conflict of interest.

10 References

Adhikari, N., Gao, J., Zhao, A., Xu, T., Chen, M., Niu, X., and Yao, T.: Spring tropical cyclones modulate near-surface isotopic compositions of atmospheric water vapour in Kathmandu, Nepal, Atmospheric Chem. Phys., 24, 3279–3296, https://doi.org/10.5194/acp-24-3279-2024, 2024.

Bonasoni, P., Laj, P., Marinoni, A., Sprenger, M., Angelini, F., Arduini, J., Bonafè, U., Calzolari, F., Colombo, T., Decesari, S., Di Biagio, C., Di Sarra, A. G., Evangelisti, F., Duchi, R., Facchini, M. C., Fuzzi, S., Gobbi, G. P., Maione, M., Panday, A., Roccato, F., Sellegri, K., Venzac, H., Verza, G. P., Villani, P., Vuillermoz, E., and Cristofanelli, P.: Atmospheric Brown Clouds in the Himalayas: First two years of continuous observations at the Nepal Climate Observatory-Pyramid (5079 m), Atmospheric Chem. Phys., 10, 7515–7531, https://doi.org/10.5194/acp-10-7515-2010, 2010.

Desilets, D.: Intensity correction factors for a cosmic ray neutron sensor (Hydroinnova Technical Document 21-02), https://doi.org/10.5281/zenodo.4569062, 2021.

https://doi.org/10.5194/egusphere-2024-1760
Preprint. Discussion started: 26 June 2024

Flückiger, E. O. and Bütikofer, R.: Swiss neutron monitors and cosmic ray research at Jungfraujoch, Adv. Space Res., 44, 1155–1159, https://doi.org/10.1016/j.asr.2008.10.043, 2009.

Gugerli, R., Salzmann, N., Huss, M., and Desilets, D.: Continuous and autonomous snow water equivalent measurements by a cosmic ray sensor on an alpine glacier, Cryosphere, 13, 3413–3434, https://doi.org/10.5194/tc-13-3413-2019, 2019.

Howat, I. M., De La Peña, S., Desilets, D., and Womack, G.: Autonomous ice sheet surface mass balance measurements from cosmic rays, Cryosphere, 12, 2099–2108, https://doi.org/10.5194/tc-12-2099-2018, 2018.

Immerzeel, W. W., Wanders, N., Lutz, A. F., Shea, J. M., and Bierkens, M. F. P.: Reconciling high-altitude precipitation in the upper Indus basin with glacier mass balances and runoff, Hydrol. Earth Syst. Sci., 19, 4673–4687, https://doi.org/10.5194/hess-19-4673-2015, 2015.

Jitnikovitch, A., Marsh, P., Walker, B., and Desilets, D.: Snow water equivalent measurement in the Arctic based on cosmic ray neutron attenuation, Cryosphere, 15, 5227–5239, https://doi.org/10.5194/tc-15-5227-2021, 2021.

Khadka, A., Brun, F., Wagnon, P., Shrestha, D., and Sherpa, T.: Surface energy and mass balance of Mera Glacier (Nepal, Central Himalaya) and their sensitivity to temperature and precipitation, https://doi.org/10.31223/x50415, 2024.

Leinss, S., Wiesmann, A., Lemmetyinen, J., and Hajnsek, I.: Snow Water Equivalent of Dry Snow Measured by Differential Interferometry, IEEE J. Sel. Top. Appl. Earth Obs. Remote Sens., 8, 3773–3790, https://doi.org/10.1109/JSTARS.2015.2432031, 2015.

Li, Y., Li, F., Shangguan, D., and Ding, Y.: A new global gridded glacier dataset based on the Randolph Glacier Inventory version 6.0, J. Glaciol., 67, 773–776, https://doi.org/10.1017/jog.2021.28, 2021.

Litt, M., Shea, J., Wagnon, P., Steiner, J., Koch, I., Stigter, E., and Immerzeel, W.: Glacier ablation and temperature indexed melt models in the Nepalese Himalaya, Sci. Rep., 9, 1–13, https://doi.org/10.1038/s41598-019-41657-5, 2019.

Masahiro Kodama, S. Kawasaki, and M. Wada: A cosmic-ray snow gauge, Int. J. Appl. Radiat. Isot., 26, 774–775, https://doi.org/10.1016/0020-708X(75)90138-6, 1975.

Masahiro Kodama, Katsuyuki Nakai, S. K.: The Determination of the Snow-Water Equivalent, J. Hydrol., 41, 85–92, 1979.

Mcjannet, D. L. and Desilets, D.: Solar Modulation Corrections for Cosmic-ray Soil and Snow Sensors Using the Global Neutron Monitor Network Solar Modulation Corrections for Cosmic-ray Soil and Snow Sensors Using the Global Neutron Monitor Network, https://doi.org/10.1002/essoar.10512737.1, 2022.

McJannet, D. L. and Desilets, D.: Incoming Neutron Flux Corrections for Cosmic-Ray Soil and Snow Sensors Using the Global Neutron Monitor Network, Water Resour. Res., 59, 1–20, https://doi.org/10.1029/2022WR033889, 2023.

Perry, L. B., Matthews, T., Guy, H., Koch, I., Khadka, A., Elmore, A. C., Shrestha, D., Tuladhar, S., Baidya, S. K., Maharjan, S., Wagnon, P., Aryal, D., Seimon, A., Gajurel, A., and Mayewski, P. A.: Precipitation Characteristics and Moisture Source Regions on Mt. Everest in the Khumbu, Nepal, One Earth, 3, 594–607, https://doi.org/10.1016/j.oneear.2020.10.011, 2020.

Shea, J. M., Wagnon, P., Immerzeel, W. W., Biron, R., Brun, F., and Pellicciotti, F.: A comparative high-altitude meteorological analysis from three catchments in the Nepalese Himalaya, Int. J. Water Resour. Dev., 31, 174–200, https://doi.org/10.1080/07900627.2015.1020417, 2015.

https://doi.org/10.5194/egusphere-2024-1760
Preprint. Discussion started: 26 June 2024

Wagnon, P., Brun, F., Khadka, A., Berthier, E., Shrestha, D., Vincent, C., Arnaud, Y., Six, D., Dehecq, A., Ménégoz, M., and Jomelli, V.: Reanalysing the 2007-19 glaciological mass-balance series of Mera Glacier, Nepal, Central Himalaya, using geodetic mass balance, J. Glaciol., 67, 117–125, https://doi.org/10.1017/jog.2020.88, 2021.

Wallace, J. M. and Hobbs, P. V.: Atmospheric Science: An Introductory Survey: Second Edition, 1–488 pp., https://doi.org/10.1016/C2009-0-00034-8, 2006.